Inorganic Chemistry

Article

pubs.acs.org/IC

Closely-Related $Zn^{II}_2Ln^{III}_2$ Complexes (Ln^{III} = Gd, Yb) with Either Magnetic Refrigerant or Luminescent Single-Molecule Magnet Properties

José Ruiz,[†] Giulia Lorusso,[⊥] Marco Evangelisti,*[,⊥] Euan K. Brechin,*[,§] Simon J. A. Pope,[‡] and Enrique Colacio*[,†]

[†]Departamento de Química Inorgánica, Facultad de Ciencias, Universidad de Granada, Av. Fuentenueva S/N, 18071 Granada, Spain

[‡]Cardiff School of Chemistry, Cardiff University, Cardiff, CF10 3AT, United Kingdom

[§]EaStCHEM School of Chemistry, The University of Edinburgh, West Mains Road, Edinburgh, EH9 3JJ, United Kingdom

[⊥]Departamento de Física de la Materia Condensada, Instituto de Ciencia de Materiales de Aragón (ICMA), CSIC-Universidad de Zaragoza, 50009 Zaragoza, Spain

Supporting Information

ABSTRACT: The reaction of the compartmental ligand *N*,*N*′,*N*″-trimethyl-*N*,*N*″-bis(2-hydroxy-3-methoxy-5-methylbenzyl)-diethylenetriamine (H_2L) with $Zn(NO_3)_2{\cdot}6H_2O$ and subsequently with $Ln(NO_3)_3{\cdot}5H_2O$ (Ln^{III} = Gd and Yb) and triethylamine in MeOH using a 1:1:1:1 molar ratio leads to the formation of the tetranuclear complexes $\{(\mu_3\text{-}CO_3)_2[Zn(\mu\text{-}L)Gd(NO_3)]_2\}{\cdot}4CH_3OH$ (**1**) and $\{(\mu_3\text{-}CO_3)_2[Zn(\mu\text{-}L)Yb(H_2O)]_2\}(NO_3)_2{\cdot}4CH_3OH$ (**2**). When the reaction was performed in the absence of triethylamine, the dinuclear compound $[Zn(\mu\text{-}L)(\mu\text{-}NO_3)Yb(NO_3)_2]$ (**3**) is obtained. The structures of **1** and **2** consist of two diphenoxo-bridged Zn^{II}–Ln^{III} units connected by two carbonate bridging ligands. Within the dinuclear units, Zn^{II} and Ln^{III} ions occupy the N_3O_2 inner and the O_4 outer sites of the compartmental ligand, respectively. The remaining positions on the Ln^{III} ions are occupied by oxygen atoms belonging to the carbonate bridging groups, by a bidentate nitrate ion in **1**, and by a coordinated water molecule in **2**, leading to rather asymmetric GdO_9 and trigonal dodecahedron YbO_8 coordination spheres, respectively. Complex **3** is made of acetate–diphenoxo triply bridged $Zn^{II}Yb^{III}$ dinuclear units, where the Yb^{III} exhibits a YbO_9 coordination environment. Variable-temperature magnetization measurements and heat capacity data demonstrate that **1** has a significant magneto–caloric effect, with a maximum value of $-\Delta S_m$ = 18.5 J kg^{-1} K^{-1} at T = 1.9 K and **B** = 7 T. Complexes **2** and **3** show slow relaxation of the magnetization and single-molecule magnet (SMM) behavior under an applied direct-current field of 1000 Oe. The fit of the high-temperature data to the Arrhenius equation affords an effective energy barrier for the reversal of the magnetization of 19.4(7) K with $\tau_o = 3.1 \times 10^{-6}$ s and 27.0(9) K with $\tau_o = 8.8 \times 10^{-7}$ s for **2** and **3**, respectively. However, the fit of the full range of temperature data indicates that the relaxation process could take place through a Raman-like process rather than through an activated Orbach process. The chromophoric L^{2-} ligand is able to act as an "antenna" group, sensitizing the near-infrared (NIR) Yb^{III}-based luminescence in complexes **2** and **3** through an intramolecular energy transfer to the excited states of the accepting Yb^{III} ion. These complexes show several bands in the 945–1050 nm region, corresponding to $^2F_{5/2} \rightarrow {}^2F_{7/2}$ transitions arising from the ligand field splitting of both multiplets. The observed luminescence lifetimes τ_{obs} are 0.515 and 10 μs for **2** and **3**, respectively. The shorter lifetime for **2** is due to the presence of one coordinated water molecule on the Yb^{III} center (and to a lesser extent noncoordinated water molecules), facilitating vibrational quenching via O–H oscillators. Therefore, complexes **2** and **3**, combining field-induced SMM behavior and NIR luminescence, can be considered to be dual magneto–luminescent materials.

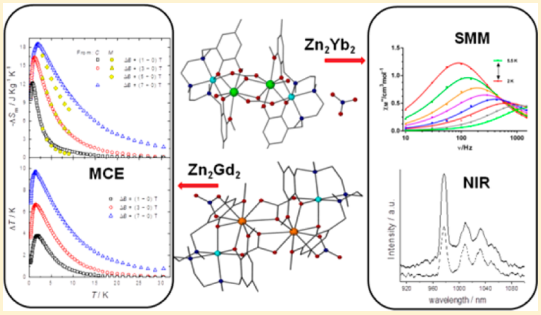

INTRODUCTION

Lanthanide coordination compounds have attracted much recent attention, in part because of their often aesthetically pleasing structures but mainly due to their fascinating and potentially applicable magnetic and photophysical properties.[1,2] Magnetochemists have focused their attention toward lanthanide-containing complexes that behave as single-molecule magnets (SMMs)[3] or low-temperature molecular magnetic coolers (MMCs).[4] SMMs are molecular complexes that can function as single-domain nanoparticles; that is to say, they exhibit slow relaxation of the magnetization and magnetic hysteresis below a blocking temperature (T_B). These chemically and physically intriguing nanomagnets have been proposed for

Received: December 18, 2013
Published: March 5, 2014

applications in molecular spintronics,[5] ultrahigh density magnetic information storage,[6] and quantum computing at the molecular level.[7] The stimulus behind the enormous increase of activity in the field of SMMs is the outlook of integrating them into nanosized devices.[8] The origin of the SMM behavior is the existence of an energy barrier (U) that prevents reversal of the molecular magnetization when the field is removed, leading to bistability.[3] To increase the height of the energy barrier and therefore to improve the SMM properties, systems with large magnetic moments and large magnetic anisotropy are required. Lanthanide complexes meet these requirements as the unpaired electrons in the inner f orbitals, which are very efficiently shielded by the fully occupied 5s and 5p orbitals and therefore interact very poorly with the ligand electrons, exhibit large and unquenched orbital angular momentum and consequently large intrinsic magnetic anisotropy and large magnetic moments in the ground state.[1] Isotropic (Gd^{III}-based) MMCs show an enhanced magneto−caloric effect (MCE), which is based on the change of magnetic entropy upon application of a magnetic field and potentially can be used for cooling applications via adiabatic demagnetisation.[4] Both lanthanide-based SMMs and MMCs are ideally characterized by a large multiplicity of the ground state, because in the former the magnetization depends on J, whereas in the latter the magnetic entropy is related to the spin s by the expression $S_m = R\ln(2s+1)$. However, the local anisotropy of the heavy Ln^{III} ions plays opposing roles in SMMs and MMCs. While highly anisotropic Ln^{III} ions favor SMM behavior, MMCs are preferably made of isotropic magnetic ions with weak exchange interactions generating multiple low-lying excited and field-accessible states, each of which can contribute to the magnetic entropy of the system, thus favoring a large MCE. Therefore, polynuclear (and high magnetic density) complexes containing the isotropic Gd^{III} ion with weak magnetic interactions between the metal ions have been shown to be appropriate candidates for MMCs.[9]

Recently, we reported the carbonate-bridged $Zn^{II}_2Dy^{III}_2$ tetranuclear complex $\{(\mu_3\text{-}CO_3)_2[Zn(\mu\text{-}L)Dy)(NO_3)]_2\}\cdot 4CH_3OH$[10a] with the compartmental ligand *N,N′,N″*-trimethyl-*N,N″*-bis(2-hydroxy-3-methoxy-5-methylbenzyl)diethylene triamine (H_2L, see Supporting Information, Figure S1), where the carbonato ligand was generated from the fixation of atmospheric CO_2 in basic medium, as has been observed for other carbonate-bridged Ln^{III}polynuclear complexes.[10b,c] This compound represents a rare example of a lanthanide-containing complex that undergoes a transformation from paramagnetic to high-energy barrier SMM under zero-field triggered only by diamagnetic dilution. In this Paper, we report two additional examples of tetranuclear complexes, $\{(\mu_3\text{-}CO_3)_2[Zn(\mu\text{-}L)Gd(NO_3)]_2\}\cdot 4CH_3OH$, hereafter named $Zn^{II}_2Gd^{III}_2$ (**1**) and $\{(\mu_3\text{-}CO_3)_2[Zn(\mu\text{-}L)Yb(H_2O)]_2\}(NO_3)_2\cdot 4CH_3OH$, hereafter named $Zn^{II}_2Yb^{III}_2$ (**2**). The former is isostructural to $\{(\mu_3\text{-}CO_3)_2[Zn(\mu\text{-}L)Dy(NO_3)]_2\}\cdot 4CH_3OH$ and exhibits ferromagnetic interaction between the metal ions and a significant MCE, whereas the latter, $\{(\mu_3\text{-}CO_3)_2[Zn(\mu\text{-}L)Yb(H_2O)]_2\}(NO_3)_2\cdot 4CH_3OH\cdot 2H_2O$, which has a similar structure minus the coordinated nitrate anions, presents SMM behavior and interesting near-infrared (NIR) luminescence properties. It is worth mentioning that NIR luminescent complexes are of high interest due to their optical, biological, and sensor applications.[11] Complexes **1** and **2** were prepared from the reaction of H_2L with $Zn(NO_3)_2\cdot 6H_2O$ and subsequently with $Ln(NO_3)_3\cdot 6H_2O$ in MeOH and triethylamine by using a 1:1:1:1 molar ratio. Colorless and yellow prismatic-shaped crystals of **1** and **2** suitable for X-ray analysis were slowly grown from the solution. When the reaction is performed in the absence of triethylamine, then the dinuclear compound $[Zn(\mu\text{-}L)(\mu\text{-}NO_3)Yb(NO_3)_2]$, hereafter named $Zn^{II}Dy^{III}$ (**3**), was obtained in the form of prismatic-shaped yellow crystals. Complexes **2** and **3** are examples of the infrequent Yb^{III} complexes showing SMM behavior.[12] Moreover, **2** and **3** show NIR luminesce and therefore can be considered to be magnetic-luminescent materials.

EXPERIMENTAL SECTION

General procedures, preparation of the complexes, physical measurements, and single-crystal structure determination details are given in the Electronic Supporting Information (ESI).

RESULTS AND DISCUSSION

The carbonato bridging ligands in compounds **1** and **2** are most likely generated, as in the case of the structurally similar complex $\{(\mu_3\text{-}CO_3)_2[Zn(\mu\text{-}L)Dy)(NO_3)]_2\}\cdot 4CH_3OH$,[10a] from the fixation of atmospheric CO_2 in basic medium. The presence of CO_3^{2-} in **1** and **2** was proved by IR spectroscopy, as these compounds exhibit, compared to **3** (prepared in the same conditions as for **2** but without using triethylamine), a new band at 1549 cm^{-1} assignable to a C−O stretching vibration of the CO_3^{2-} anion.

We begin by discussing the simpler dinuclear complex **3**. This compound is isostructural with two $M^{II}Dy^{III}$ (M^{II} = Ni and Co) complexes previously reported by us,[10a,13] and its structure consists of a dinuclear $Zn^{II}Yb^{III}$ molecule in which the Yb^{III} and Zn^{II} ions are bridged by two phenoxo groups of the L^{2-} ligand and one μ-nitrate anion (Figure 1).

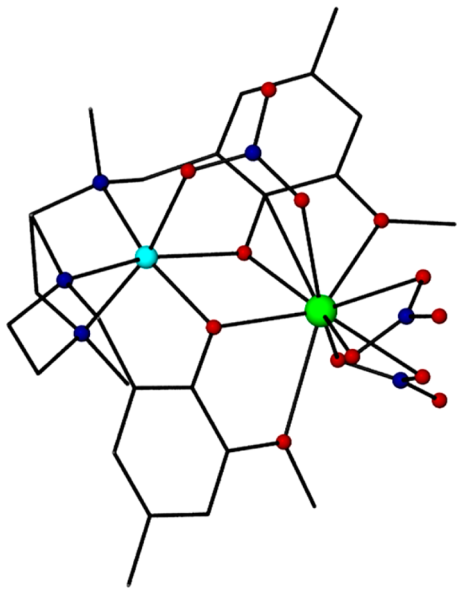

Figure 1. Perspective view of complex **3**. Color code: N = blue, O = red, Zn = light blue, Yb = green, C = black.

The L^{2-} ligand coordinates the Zn^{II} ions in such a way that the three nitrogen atoms, and consequently the three oxygen atoms, occupy fac positions on the slightly trigonally distorted ZnN_3O_3 coordination polyhedron. The Yb^{III} ion exhibits a YbO_9 coordination sphere that is made by the two phenoxo bridging oxygen atoms, the two methoxy oxygen atoms, one

dx.doi.org/10.1021/ic403097s | Inorg. Chem. 2014, 53, 3586−3594

oxygen atom from the nitrate bridging group, and four oxygen atoms belonging to two bidentate nitrate anions. The Yb−O distances are in the range of 2.176−2.571 Å, thus indicating a high degree of distortion in the YbO_9 coordination sphere. The calculation of the degree of distortion of the YbO_9 coordination polyhedron with respect to ideal nine-vertex polyhedra was performed by using continuous shape-measure theory and SHAPE software (see Supporting Information, Table S4).[14] The calculation showed that the YbO_9 coordination polyhedron is intermediate between several ideal polyhedra, the lowest continuous measures being those of capped square antiprism, C_{4v} (1.45), muffin, C_s (1.58), and tricapped trigonal prism, D_{3h} (2.26). The bridging fragment is also rather asymmetric, with different bond angles and distances involving the Yb^{III} and Zn^{II} metal ions. The bridging nitrate group forces the structure to be folded with the average hinge angle of the $Zn(\mu\text{-}O_2)Dy$ bridging fragment being 14.81° and the average Zn−O−Yb angle of 106.04°. The intradinuclear Zn−Yb distance is 3.438 Å.

Complex **1** is isostructural with the previously reported complex $\{(\mu_3\text{-}CO_3)_2[Zn(\mu\text{-}L)Dy(NO_3)]_2\}\cdot 4CH_3OH$[10a] and exhibits a centrosymmetric tetranuclear structure (see Figure 2 and Supporting Information, Tables S2 and S3 for crystallographic details and selected bond angles and distances) that consists of two diphenoxo-bridged $[Zn(\mu\text{-}L)Gd(NO_3)]$ dinuclear units connected by two tetradentate carbonato bridging ligands acting with a μ_3−κ^2-O,O′:κ-O′:κ-O″ coordination mode, giving rise to a rhomboidal $Gd(O)_2Gd$ bridging unit with a Gd−O−Gd bridging angle of 115.6° and two different Gd−O distances of 2.385 and 2.435 Å, respectively.

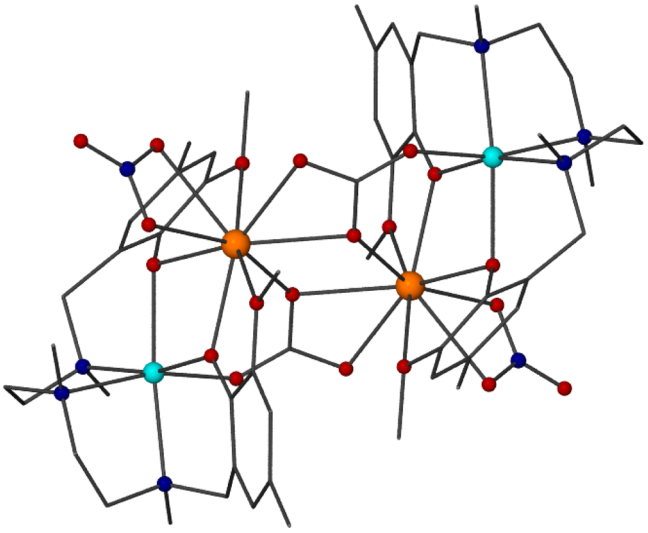

Figure 2. Perspective view of the structure of **1**. Color code: N = dark blue, O = red, Zn = light blue, Gd = orange, C = gray. Hydrogen atoms and solvent molecules have been omitted for clarity.

The Gd^{III} ion exhibits a rather asymmetric GdO_9 coordination sphere that is made from the two phenoxo bridging oxygen atoms, the two methoxy oxygen atoms, three oxygen atoms from the carbonato bridging groups, and two oxygen atoms belonging to a bidentate nitrate anion. The latter and the chelating part of the carbonato ligand occupy cis positions in the Gd^{III} coordination sphere. The Gd−O distances are in the range of 2.302−2.564 Å. In the bridging fragment, the $Gd(O)_2Gd$ and carbonato planes are not coplanar, exhibiting a dihedral angle of 26.37°. The intratetranuclear Gd···Gd and Gd···Zn distances are 4.079 and 3.509 Å, respectively.

The tetranuclear molecules $\{(\mu_3\text{-}CO_3)_2[Zn(\mu\text{-}L)Gd(NO_3)]_2\}$ are well-separated in the structure by methanol molecules of crystallization, the shortest Gd···Gd distance being 8.369 Å. One of the methanol molecules forms bifurcated hydrogen bonds with one of the oxygen atoms of the chelating part of the carbonato ligand and the oxygen atom of a second methanol molecule, with donor−acceptor distances of 2.661 and 2.692 Å, respectively.

The structure of **2** is also centrosymmetric and very similar to that of **1**, but it has a water molecule coordinated to the Yb^{III} ion instead of a bidentate nitrate ion (Figure 3). This change is probably due to the significant size reduction on going from Gd^{III} to Yb^{III} as a consequence of the lanthanide contraction. In fact the $Ln-O_{carbonate}$ distances in the $Ln(O)_2Ln$ fragment are reduced from 2.435 and 2.385 Å in **1** to 2.327 and 2.302 Å in **2**, with the Yb−O−Yb angles in the bridging fragment increasing to 114.0 Å. Therefore, the smaller size of the Yb^{III} favors the adoption of an eight-coordinated YbO_8 coordination polyhedron instead of a nine-coordinated one. The degree of distortion of the YbO_8 coordination polyhedron with respect to ideal eight-vertex polyhedra was calculated by using the continuous shape-measure theory and SHAPE software (see Supporting Information, Table S4).[14] The calculation indicated that the YbO_8 coordination polyhedron is intermediate between several ideal polyhedra, those being triangular dodecahedron D_{2d}, biaugmented trigonal prism C_{2v}, and square-antiprism D_{4d}. Shape measures relative to ideal triangular dodecahedron are however by far the lowest, with a value of 1.54 (see Supporting Information, Figure S2).

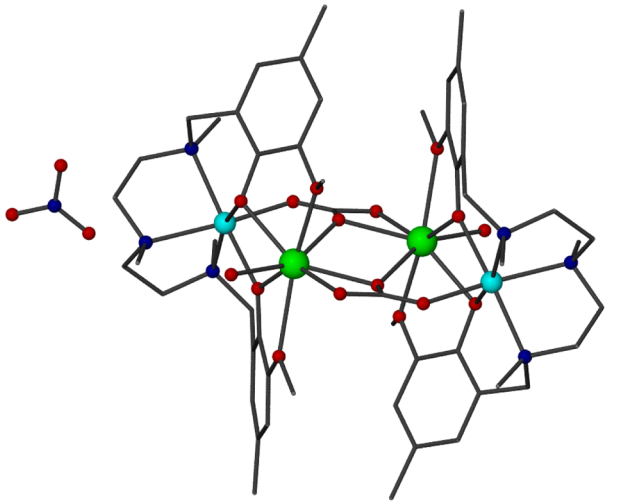

Figure 3. Perspective view of the structure of **2**. Color code: N = blue, O = red, Zn = light blue, Yb = green, C = gray. Hydrogen atoms and solvent molecules have been omitted for clarity.

The YbO_8 coordination polyhedron can also be described as trigonal bipyramidal, in which the phenol oxygen atoms are above and below the pentagonal plane. The rest of the structure is similar to that of **1**, but all distances involving the Yb^{III} ions are shorter, as expected. Thus, the Yb−O distances are in the range of 2.176−2.571 Å, whereas the intratetranuclear Yb···Yb and Yb···Zn distances are 3.884 and 3.449 Å, respectively. The shortest Yb−O distances correspond to the $Yb-O_{phenol}$ and

dx.doi.org/10.1021/ic403097s | Inorg. Chem. 2014, 53, 3586−3594

Yb−O_{water} distances. The coordinated water molecules of the tetranuclear $Zn^{II}_2Yb^{III}_2$ cations, the molecules of methanol, the noncoordinated water molecules, and the nitrate anions are involved in hydrogen bonds to form chains with donor−acceptor distances in the range of 2.603−2.969 Å, the lowest intrachain and interchain distances being 10.009 and 10.198 Å, respectively.

MAGNETIC PROPERTIES

The temperature dependence of the $\chi_M T$ product for **1** is shown in Supporting Information, Figure S3. The room-temperature $\chi_M T$ value for **1** (15.71 cm^3 K mol^{-1}) agrees with the expected value for a pair of noninteracting Gd^{III} (s = 7/2) ions (15.75 cm^3 K mol^{-1} with g = 2). On lowering the temperature, $\chi_M T$ remains approximately constant to 30 K and then abruptly increases, reaching a value of 21.3 cm^3 K mol^{-1} at 2 K.

This behavior is due to an intra-dinuclear ferromagnetic interaction between the Gd^{III} ions. The magnetic properties have been modeled using the following spin Hamiltonian:

$$H = -JS_{Gd1}S_{Gd2} + g\mu_B(S_{Gd1} + S_{Gd2})B$$

where J is the isotropic exchange interaction, g is the g factor, μ_B the bohr magneton and **B** the applied magnetic field. The best fit of the experimental susceptibility afforded the following set of parameters: J = +0.038(2) cm^{-1} and g_{Gd} = 2.02(4). The field dependence of the isothermal magnetization (M) between 2 and 10 K is shown in Figure 4. The calculated isothermal

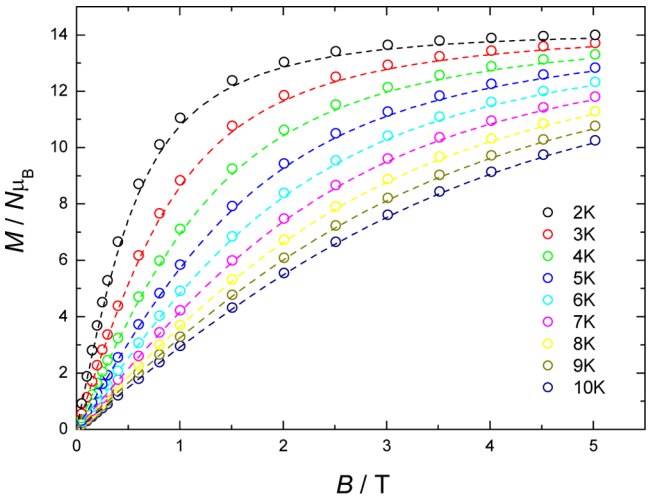

Figure 4. (○) Experimental isothermal magnetization data from T = 2 to 10 K, as labeled (dashed lines). Calculated curves for two Gd^{III} ions interacting ferromagnetically with J = 0.038 cm^{-1}.

magnetization curves using the J and g values obtained from fitting the susceptibility data (depicted as dashed lines in Figure 5) nicely agree with the experimental data (open circles (○)).

Figure 5 shows the temperature dependence of the molar heat capacity C/R, measured in the presence of several magnetic fields. The lattice contribution (dashed line in the top panel), which we associate with vibrational phonon modes, develops at high temperature. Using the Debye model, we have obtained a Debye temperature θ_D of 36 K,which falls within the range of values usually found for this type of system.[15] The applied (**B**) and exchange field participate concomitantly and split the S = 7/2 spin multiplet of each Gd^{III} ion, resulting in

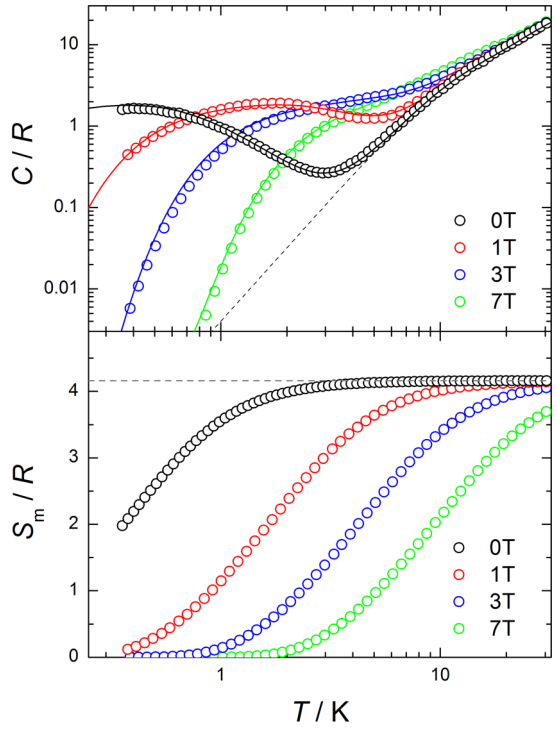

Figure 5. (top, ○) Molar heat capacity for Zn_2Gd_2(**1**) for several applied magnetic fields, as labeled. (solid lines) Theoretical calculations for heat capacity, sum of lattice (dashed line) and magnetic contribution, obtained as explained in the text. (bottom) Magnetic entropy obtained from heat capacity data. (dashed line) The limit given by the spin degrees of freedom involved.

typical Schottky-like contributions. The exchange is taken into account by considering a local field B_{loc}, added to **B**. From the best fit of the experimental data (solid lines) we obtain B_{loc} = 0.28 T. Since $g\mu_B s B_{loc} = Js^2$ (with $s = 2s_{Gd}$) we obtain J = 0.037 cm^{-1}, in perfect agreement with the value found from the fit of the susceptibility.

From the magnetic contribution of the heat capacity C_m, obtained by subtracting from C the lattice contribution (dashed line in Figure 5), we derive the magnetic entropy for **1** as a function of temperature and field (Figure 5, bottom) by making use of the equation

$$S_m(T, B) = \int_0^T \frac{C_m(T, B)}{T} dT$$

The lack of data in the zero-field heat capacity for temperatures lower than 0.3 K was corrected by rescaling the experimental entropy such that the high-temperature limit meets the value corresponding to the full magnetic entropy content per mole, that is, $2R\ln(s_{Gd} + 1) = 4.16R$ for s_{Gd} = 7/2 (dashed line in the bottom panel of Figure 5).

From the obtained entropy curves we finally calculate the magnetic entropy change ΔS_m and the adiabatic temperature change ΔT_{ad}, respectively, reported in the top and bottom panels of Figure 6. The ΔS_m was also estimated from the experimental magnetization data (yellow full markers) by making use of the Maxwell relation

$$\Delta S_m(T, \Delta B) = \int_{B_i}^{B_f} \left[\frac{\partial M(T, B)}{\partial T}\right]_B dB$$

dx.doi.org/10.1021/ic403097s | Inorg. Chem. 2014, 53, 3586−3594

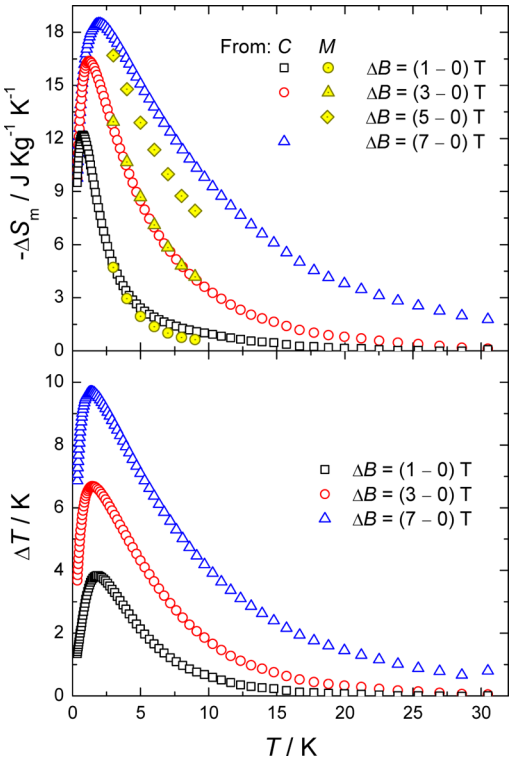

Figure 6. (top) Magnetic entropy change for the labeled magnetic field changes, as obtained from the heat capacity and isothermal magnetization curves. (bottom) Adiabatic temperature change for the corresponding labeled magnetic field changes.

The magnetic entropy changes, independently found from heat capacity and magnetization experiments, are in good agreement, thus confirming the validity of our data analyses. The maximum value of $-\Delta S_m$ achieved for **1** is 18.5 J kg^{-1} K^{-1} at T = 1.9 K and applied field change of ΔB = 7 T, while ΔT_{ad} increases up to 9.6 K at T = 1.4 K and ΔB = 7 T.

The MCE observed for **1** is lower than that found for the complex $[\{Gd(OAc)_3(H_2O)_2\}_2]\cdot 4H_2O$[16] ($-\Delta S_m$ = 40.6 J kg^{-1}K^{-1} for ΔB = 7 T) that has a similar bridging fragment between the Gd^{III} ions, but using acetate instead of carbonate bridging ligands. This is as expected since the MCE is directly correlated to the molar mass, and the former have a much lower magnetic density than the latter. At such large applied fields, sufficient for magnetically decoupling all spin centers, the MCE of Gd^{III}-based complexes is exclusively determined by the values of the molar mass, indeed.[9g] For both complexes, the observed maximum $-\Delta S_m$ values are nearly as large as the full entropy content per mole that corresponds to $2R\ln(2s_{Gd} + 1) = 4.16R$, which is equivalent to 20.3 J kg^{-1}K^{-1} and 42.5 J kg^{-1}K^{-1} for **1** and $[\{Gd(OAc)_3(H_2O)_2\}_2]\cdot 4H_2O$, respectively. The $-\Delta S_m$ value for **1** is somewhat lower than those observed for other Gd_2 complexes[9a,b] but is significantly lower than those reported for magnetic dense Gd_n[9c−f] clusters and one-dimensional to three-dimensional polymeric complexes,[9g−n] with values as high as 46.1 J kg^{-1} K^{-1}[9e] and 59 J kg^{-1}K^{-1},[9m] respectively.

The magnetic properties of complexes **2** and **3** are given in the form of $\chi_M T$ versus T in Supporting Information, Figure S4. The room-temperature $\chi_M T$ values of complexes **2** and **3** are 5.09 cm^3 mol^{-1} K and 2.51 cm^3 mol^{-1} K, respectively, which are in rather good agreement with the expected theoretical values using the free ion approximation (5.14 and 2.57 cm^3 mol^{-1} K) for two noninteracting Yb^{III} ions and one isolated Yb^{III} ion, respectively ($^2F_{7/2}$, S = 1/2, L = 3, g = 8/7). The $\chi_M T$ product for **2** steadily decreases with decreasing temperature, reaching a minimum value of 3.48 cm^3 mol^{-1} K at 5 K, and then slightly increases upon cooling, reaching 3.56 cm^3 mol^{-1} K at 2 K. The increase below 5 K could be due either to the effect of the crystal field or to the presence of a weak ferromagnetic interaction as previously observed for **1**. For complex **3**, the $\chi_M T$ product continuously decreases with temperature to reach a value of 1.67 cm^3 mol^{-1} K. The decrease is due to the effects of the thermal depopulation of the m_J sublevels of the $^2F_{7/2}$ ground multiplet of the Yb^{III} ion, as split by the crystal field.

We have tried to model the magnetic properties of **2** and **3** taking into account the crystal-field effects that split the ground $^2F_{7/2}$ term of the Yb^{III} Kramers ion in J + 1/2 doublets and the exchange coupling between the ground doublets. In keeping with the trigonal dodecahedron D_{2d} local symmetry of the YbO_8 coordination environment, the Crystal Field Hamiltonian, H_{CF}, to be considered is

$$H_{CF} = \sum_{i=1}^{2} (B_2^0\mathbf{O_2^0} + B_4^0\mathbf{O_4^0} + B_6^0\mathbf{O_6^0} + B_4^4\mathbf{O_4^4} + B_6^4\mathbf{O_6^4}) - 2J(\mathbf{J}_1 + \mathbf{J}_2) + \beta g_J(\mathbf{J}_1 + \mathbf{J}_2)$$

where the first term is the crystal field component expressed as Steven's equivalent operators ($\boldsymbol{O_k^q}$), which are a function of the total angular momentum matrices associated with the $^2F_{7/2}$ term. The second and third terms correspond to the exchange coupling and Zeeman components, respectively. The direct-current (dc) magnetic susceptibility of **1** was simulated with the program PHI.[17] However, the large number of parameters makes it impossible to find a unique solution, even if only the B_2^0, B_4^0, and B_6^0 CF parameters are considered. Nevertheless, from the different simulations using different CF parameters, with and without consideration of the exchange coupling between the ground doublets, the following conclusions can be drawn: (a) the susceptibility data can be simulated by using only B_2^0, B_4^0, and B_6^0 CF parameters without considering the exchange between the Yb^{III} ions. (b) The ground doublet is the M_J = ±7/2. The first excited state, M_J = ±1/2 being located at an energy of <1 cm^{-1} above the ground state, with the other two M_J states are located at ~250 cm^{-1} (M_J = ±3/2) and ~410 cm^{-1} (M_J = ±5/2). A similar crystal field splitting of the $^2F_{7/2}$ multiplet has been recently reported for another centrosymmetric dinuclear Yb^{III} complex with carboxylate bridging ligands that, like **2**, exhibits a YbO_8 coordination environment in a trigonal dodecahedron geometry and very similar average Yb−O distances.[12]

Although the YbO_9 coordination environment of **3** is rather asymmetric, the dc susceptibility data could be simulated with a high-symmetry Hamiltonian that employs just three CF parameters (B_2^0, B_4^0, and B_6^0), leading to an M_J = ±7/2 ground state, which is nearly degenerate with the M_J = ±1/2 (the energy separation is <0.1 cm^{-1}). The other two M_J states would be located at ~240 cm^{-1} (M_J = ±3/2) and ~400 cm^{-1} (M_J = ±5/2). The average Yb−O distances for compound **3** (2.36 Å), being slightly larger than that for compound **2** (2.32 Å), may be responsible for the weaker crystal field splitting in **3**.

UV and NIR luminescence spectra of mononuclear SMMs have been used to determine the energy levels of the Ln^{III} ions allowing comparison of these levels to those obtained from magnetic data or ab initio calculations.[10b,12,18] This method-

dx.doi.org/10.1021/ic403097s | Inorg. Chem. 2014, 53, 3586−3594

ology has proven to be very useful, particularly in the case of Dy^{III} and Tb^{III} SMMs.[18] Recently, it has been shown that the compartmental L^{2-} ligand, as well as their Schiff-base counterparts, are able to act as an "antenna" group, sensitizing Ln^{III}-based luminescence through an intramolecular energy transfer to the excited states of the accepting Ln^{III} ion.[10a,19] In view of this, and with the aim of obtaining the energy gap between the ground and first excited states of compounds **2** and **3**, we analyzed the photophysical properties of microcrystalline samples of these complexes at room temperature and at 77 K. Excitation of the complexes at 300 and 350 nm resulted in the observation of sensitized characteristic Yb^{III} emission in the NIR region. Note that the emission spectrum of **2** (Figure 7) at both room temperature and at 77 K exhibits three relatively well-defined bands at 976, 1008, and 1031 nm and a possible weaker feature at ca. 1045 nm.

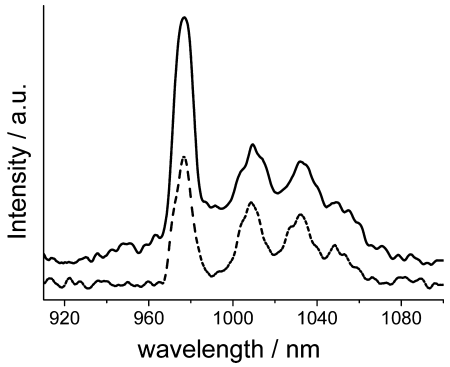

Figure 7. Solid NIR-emission spectra of **2** (λ_{exc} = 350 nm) at room temperature (solid line) and at 77 K (dashed line).

It is possible that two different assignments of the above transitions could be made: (a) the observed bands may correspond to the four components expected from the $^2F_{5/2}\rightarrow{}^2F_{7/2}$ transition arising from the ligand field splitting of the $^2F_{7/2}$ multiplet. Although the position of the emission bands and consequently the energy gap between the ground and first excited state ~315 cm^{-1} and the total splitting ~665 cm^{-1} are similar to those found for the ytterbium-doped $Li_6Y(BO_3)_3$ compound[20] (where the Yb^{III} ion also exhibits a YbO_8 coordination environment), these values are larger than those usually calculated and observed for other YbO_8 complexes.[12] In addition to this, an argument against this assignment is that the energy gap between the ground and first excited state would be exceedingly larger than the energy gap calculated from the simulation of the dc susceptibility data with the above crystal-field Hamiltonian. (b) Alternatively, the two most energetic transitions are very close in energy and appear together as the band at 976 nm. This assignment is more in line with the energy gap calculated from the dc susceptibility data (<2 cm^{-1}), and the total crystal-field splitting of the $^2F_{7/2}$ multiplet (550 cm^{-1}) is in agreement with those observed for other YbO_8 complexes.[12] It is worth mentioning that other YbO_8 complexes with triangular dodecahedron geometry and similar Yb−O distances do not exhibit the low-energy band at ~1050 nm. (The other three bands appear at almost the same energies as in the emission spectrum of **2**.) Although its origin is unclear, the apparent weak band at the lowest energy (1045 nm) could be tentatively attributed to, among other things, the crystal growth process leading to the creation of different Yb^{III} defects in the polycrystalline sample, or to a strong interaction of the Yb^{III} ion with lattice vibrations, which would result in additional vibronic transitions in the spectra, or to local Yb^{III}−Yb^{III} interactions inducing modifications in the crystal-field splitting of the $^2F_{7/2}$ ground multiplet.[20] In view these considerations it is reasonable to assume that the second assignment (b) is more probable.

The appearance of the room-temperature emission spectrum of compound **3** shows a well-resolved structure (Supporting Information, Figure S5). The emission profile can be deconvoluted into seven bands in the 948−1045 nm range and attributed to the $^2F_{5/2}\rightarrow{}^2F_{7/2}$transitions. At 77 K the high-energy bands observed in the room-temperature emission spectrum at 948 and 962 nm disappear and therefore are attributed to "hot" bands, arising from thermally populated high crystal field levels of the $^2F_{5/2}$ state. Although bands at 977 and 992 nm undergo a decrease in intensity in relation to the lower-energy bands, the former is observed in all reported Yb^{III} complexes and therefore cannot be considered as a hot band. However, the band at 992 nm does not usually appear in Yb^{III} complexes and when observed is assigned to a hot band.[12] The remaining bands (977, 1010, 1024, and 1043 nm) are assigned as in complex **2**, so that the band at 977 nm encompasses the two more energetic bands whose difference represents the energy gap between the ground and first excited doublets of the $^2F_{7/2}$ ground multiplet. This assignment is also in good agreement with the dc magnetic results. It is worth mentioning that the $[Zn(\mu\text{-}L)(\mu\text{-}OAc)Yb(NO_3)_2]$ complex,[19b] whose structure is very similar to that of compound **3**, but having an acetato bridge between the Zn^{II} and Yb^{III} metal ions, does not exhibit the band at about 1040 nm, which could support the above-suggested origin of this band (crystal defects, vibronic transitions, and Yb^{III}−Yb^{III} interactions).

Luminescence decay profiles were satisfactorily fitted with single exponential functions in both cases, thus indicating the existence of only one emissive Yb^{III} center in **2** and **3**, (in **2** there are two Yb^{III} centers, but they are crystallographically equivalent). The observed luminescence lifetimes (τ_{obs}) are 0.515 and 10 μs for **2** and **3**, respectively. In the case of **2**, the presence of one coordinated water molecule to the Yb^{III} center (and to a lesser extent noncoordinated water molecules) favors vibrational quenching via O−H oscillators, and is expected to exhibit a relatively shorter lifetime.[21] In contrast, for complex **3** the effective encapsulation of the metal ion, and thus complete absence of coordinated and noncoordinated solvent molecules, should largely reduce the quenching of the Yb^{III} center, and a relatively long lifetime is observed.

Dynamic alternating-current (ac) magnetic susceptibility measurements as a function of both temperature and frequency were performed on **2** and **3**. These complexes did not show any out-of-phase ($\chi_{M''}$) signal under zero external field, which can be attributed to the presence of fast relaxation of the magnetization via a quantum tunneling of magnetization (QTM) mechanism typical of 4f-containing complexes.[1] When the ac measurements were performed in the presence of a small external dc field of 1000 G to fully or partly suppress the quantum tunneling relaxation of the magnetization, complexes **2** and **3** showed typical SMM behavior below 8 K with out-of-phase peaks in the 5K (1488 Hz)−4K (575 Hz) and 5.5K (1490 Hz)−3.5K (100 Hz) ranges, respectively (see Figures 8 and 9). Despite the fact that dc fields higher than 1000 Oe do not additionally slow the relaxation of the magnetization, both $\chi_{M'}$ and $\chi_{M''}$ components (Figures 8 and 9 top) do not go to zero below the maxima at low temperature,

dx.doi.org/10.1021/ic403097s | Inorg. Chem. 2014, 53, 3586−3594

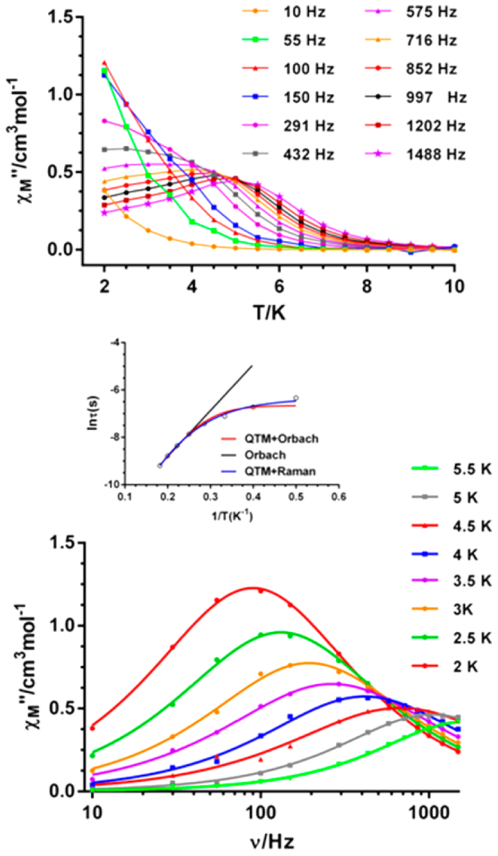

Figure 8. Temperature dependence of the molar out-of-phase ac susceptibility (χ_M'') for **2** under 1000 Oe dc applied field at different frequencies (top). Frequency dependence of the molar out-of-phase ac susceptibility (χ_M'') for **2** under 1000 Oe dc applied field at different temperatures (bottom). Solid lines represent the best fitting of the experimental data to the Debye model. (inset) Arrhenius plots of relaxation times of **2** under 1 kOe. (black line) The best fitting of the experimental data to the Arrhenius equation. (red line) The best fit to a QTM + Orbach relaxation process. (blue line) The best fit to a QTM + Raman relaxation process.

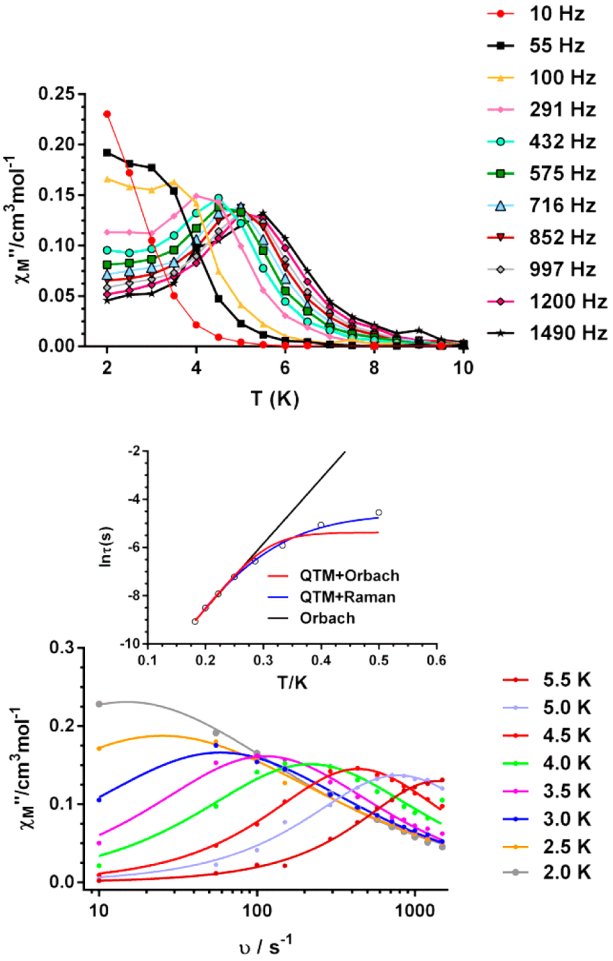

Figure 9. Temperature dependence of the molar out-of-phase ac susceptibility (χ_M'') for **3** under 1000 Oe dc applied field at different frequencies (top). Frequency dependence of the molar out-of-phase ac susceptibility (χ_M'') for **3** under 1000 Oe dc applied field at different temperatures (bottom). Solid lines represent the best fitting of the experimental data to the Debye model. (inset) Arrhenius plots of relaxation times of **3** under 1 kOe. (black lines) The best fitting of the experimental data to the Arrhenius equation. (red line) The best fit to a QTM + Orbach relaxation process. (blue line) The best fit to a QTM + Raman relaxation processes.

which can be taken as a clear indication that the QTM has not been efficiently suppressed, which can be promoted by transverse anisotropy and by dipolar and hyperfine interactions. Although for Kramers ions, such as Yb^{III}, the first mechanism would not facilitate the QTM relaxation process, it might be favored by the mixture of the wave function of the ground doublet with that of excited-state doublets via the crystal field.[22]

The Cole−Cole plots (Supporting Information, Figures S6 and S7) show, in the high-temperature regions (6−4 K and 5−4 K for **2** and **3**, respectively), semicircular shapes with α values in the ranges of 0.02−0.09 and 0.03−0.1 for **2** and **3**, respectively, thus indicating the presence of a very narrow distribution of slow relaxation in that region. Below 4 K, the α values undergo a fast increase with decreasing temperature, pointing to the presence of multiple relaxation processes. This is expected as in the low-temperature region the fast QTM relaxation process begins to be dominant.

The frequency dependence of χ_M'' at each temperature was fitted to the generalized Debye model, which permits the relaxation time τ to be extracted. The results were then used in constructing the Arrhenius plots for **2** and **3**, which are shown in the inset of Figures 8 and 9. The fit of the high-temperature data (above 4 and 3.5 K for **2** and **3**, respectively) afforded an effective energy barrier for the reversal of the magnetization of 19.4(7) K with $\tau_o = 3.1 \times 10^{-6}$ s and 27.0(9) K with $\tau_o = 8.8 \times 10^{-7}$ s, for **2** and **3**, respectively. The Arrhenius plots, constructed from the temperatures and frequencies of the maxima observed for the χ_M'' signals in Figures 8 and 9 (top), lead to the same results, as expected.

The energy barriers extracted for **2** and **3** from ac dynamic susceptibility measurements are larger than the corresponding energy gap between the ground and first excited doublet states determined by dc susceptibility measurements, which can be due to an underestimation of the energy gaps by the simple crystal-field model we used to fit the dc data. Nevertheless, the excellent fit of the ac susceptibility data to a combination of Raman and QTM processes (Figures 8 and 9 and Electronic Supporting Information) might indicate that the spin−lattice relaxation is not of the thermally activated type but takes place through an optical−acoustic Raman-like process. Note that Raman relaxation processes have previously been proposed for Yb^{III} complexes.[12]

dx.doi.org/10.1021/ic403097s | Inorg. Chem. 2014, 53, 3586−3594

CONCLUSIONS

By deliberately designing a N_3O_4 compartmental ligand (N_3O_2 inner site and O_4 outer site) we have succeeded in obtaining two closely related $Zn^{II}_2Ln^{III}_2$ tetranuclear complexes (Ln = Gd and Yb), in which two carbonate bridging ligands connect two diphenoxo-bridged $Zn^{II}Ln^{III}$ units and a simpler diphenoxo-bridged dinuclear $Zn^{II}Yb^{III}$ complex. The $Zn^{II}_2Gd^{III}_2$ complex exhibits a weak ferromagnetic interaction between the Gd^{III} ions through the carbonato bridging ligands and a significant magneto-caloric effect. The $Zn^{II}_2Yb^{III}_2$ and $Zn^{II}Yb^{III}$ complexes show field-induced SMM behavior, with the relaxation of the magnetization on the Yb^{III} centers taking place through a Raman-like process rather than through an activated Orbach process. These two compounds are rare examples of Yb^{III}-containing SMMs. Moreover, both $Zn^{II}_2Yb^{III}_2$ and $Zn^{II}Yb^{III}$ exhibit luminescence in the NIR region, the lifetime being shorter for the former, which is due to the presence of one water molecule coordinated to the Yb^{III} center (and to a lesser extent noncoordinated water molecules) allowing vibrational quenching via O−H oscillators. Therefore, the $Zn^{II}_2Yb^{III}_2$ and $Zn^{II}Yb^{III}$ complexes reported here can be considered as dual magneto−luminescence materials combining NIR emission and field-induced SMM behavior.

ASSOCIATED CONTENT

Supporting Information

This includes experimental procedures, elemental analyses for all the complexes, X-ray crystallographic data for **1**−**3**, including data collection, refinement, and selected bond lengths and angles. Shape measures, dc susceptibility data, variable-frequency temperature dependence of the ac in-phase χ_M' signal, and Cole−Cole plots for complexes **2** and **3** are also included. This material is available free of charge via the Internet at http://pubs.acs.org.

AUTHOR INFORMATION

Corresponding Authors

*E-mail: evange@unizar.es (M.E.).
*E-mail: ebrechin@staffmail.ed.ac.uk (E.K.B.).
*E-mail: ecolacio@ugr.es (E.C.).

Notes

The authors declare no competing financial interest.

ACKNOWLEDGMENTS

Financial support from Ministerio de Economía y Competitividad (MINECO) for Projects CTQ-2011-24478 and MAT2012-38318-C03-01, the Junta de Andalucía (FQM-195 and the Project of Excellence P11-FQM-7756), and the University of Granada is acknowledged. E.K.B. thanks the EPSRC for funding. S.J.A.P. thanks Cardiff University and the EPSRC. G.L. acknowledges EU for a Marie Curie IEF (PIEF-GA-2011-299356). We are grateful to Nuria Clos, Unitat de Mesures Magnètiques Centers Científics i Tecnològics, Universitat de Barcelona, Spain. Technical and human support provided by SGIker (UPV/EHU, MINECO, GV/EJ, ERDF, and ESF) for X-Ray measurements is gratefully acknowledged. We thank Dr. J. M. Herrera, Universidad de Granada, for his help with the emission spectra deconvolution.

REFERENCES

(1) (a) Rinehart, J. D.; Long, J. R. *Chem. Sci.* **2011**, *2*, 2078−2085. (b) Sorace, L.; Benelli, C.; Gatteschi, D. *Chem. Soc. Rev.* **2012**, *42*, 3278−3288. (c) Luzon, J.; Sessoli, R. *Dalton Trans.* **2012**, *41*, 13556−13567. (d) Clemente-Juan, J. M.; Coronado, E.; Gaita-Ariño, A. *Chem. Soc. Rev.* **2012**, *41*, 7464−7478.

(2) (a) Ward, M. D. *Coord. Chem. Rev.* **2007**, *251*, 1663−1677. (b) Binnemans, K. *Coord. Chem. Rev.* **2009**, *109*, 4283−4374. (c) Bünzli, J.-C. G. *Acc. Chem. Res.* **2006**, *39*, 53−61. (d) Bünzli, J.-C. G. *Acc. Chem. Res.* **2006**, *39*, 53−61.

(3) Gatteschi, D.; Sessoli, R.; Villain, J. *Molecular Nanomagnets;* Oxford University Press: Oxford, UK, 2006.

(4) (a) Evangelisti, M.; Brechin, E. K. *Dalton Trans.* **2010**, *39*, 4672−4676. (b) Sessoli, R. *Angew. Chem., Int. Ed.* **2012**, *51*, 43−45. (c) Sharples, J. W.; Collison, D. *Polyhedron* **2013**, *54*, 91−103.

(5) Bogani, L.; Wernsdorfer, W. *Nat. Mat.* **2008**, *7*, 179−186.

(6) (a) Rocha, A. R.; García-Suárez, V. M.; Bailey, S. W.; Lambert, C. J.; Ferrerand, J.; Sanvito, S. *Nat. Mater.* **2005**, *4*, 335−339. (b) Affronte, M. *J. Mater. Chem.* **2009**, *19*, 1731−1737.

(7) (a) Leuenberger, M. N.; Loss, D. *Nature* **2001**, *410*, 789−793. (b) Ardavan, A.; Rival, O.; Morton, J. J. L.; Blundell, S. J.; Tyryshkin, A. M.; Timco, G. A.; Winpenny, R. E. P. *Phys. Rev. Lett.* **2007**, *98*, 057201. (c) Stamp, P. C. E.; Gaita-Ariño, A. *J. Mater. Chem.* **2009**, *19*, 1718−1730.

(8) (a) Candini, A.; Klyatskaya, S.; Ruben, M.; Wernsdorfer, W.; Affronte, M. *Nano Lett.* **2011**, *11*, 2634−2639. (b) Vincent, R.; Klyatskaya, S.; Ruben, M.; Wernsdorfer, W.; Balestro, F. *Nature* **2012**, *488*, 357−360. (c) Ganzhorn, M.; Klyatskaya, S.; Ruben, M.; Wernsdorfer, W. *Nature Nanotechnology* **2013**, *8*, 165−169. (d) Jenkins, M.; Hümmer, T.; Marínez-Pérez, M. J.; García-Ripoll, J.; Zueco, D.; Luis, F. *New. J. Phys.* **2013**, *15*, 095007.

(9) (a) Guo, F. S.; Leng, J. D.; Liu, J. L.; Meng, Z. S.; Tong, M. L. *Inorg. Chem.* **2012**, *51*, 405−413. (b) Sedláková, L.; Hankoa, J.; Orendáčová, A.; Orendáč, M.; Zhou, C.-L.; Zhu, W.-H.; Wang, B.-W.; Wang, Z.-M.; Gao, S. *J. Alloys Compd.* **2009**, *487*, 425−429. (c) Sharples, J. W.; Zheng, Y.-Z.; Tuna, F.; McInnes, E. J. L.; Collison, D. *Chem. Commun.* **2011**, *47*, 7650−7652. (d) Guo, F. S.; Chen, Y. C.; Mao, L. L.; Lin, W. Q.; Leng, J. D.; Tarasenko, R.; Orendáč, M.; Prokleška, J.; Sechovský, V.; Tong, M. L. *Chem.—Eur. J.* **2013**, *19*, 14876−14885. (e) Chang, L. X.; Xiong, G.; Wang, L.; Cheng, P.; Zhao, B. *Chem. Commun.* **2013**, *49*, 1055−1057. (f) Wu, M.; F. Jiang, F.; Kong, X.; Yuan, D.; Long, L.; Al-Thabaiti, S. A.; Hong, M. *Chem. Sci.* **2013**, *4*, 73104−73109. (g) Lorusso, G.; Palacios, M. A.; Nichol, G. S.; Brechin, E. K.; Roubeau, O.; Evangelisti, M. *Chem. Commun.* **2012**, *48*, 7592−7594. (h) Chen, Y. C.; Guo, F. S.; Zhen, Y. Z.; Liu, J. L.; Leng, J. D.; Tarasenko, R.; Orendáč, M.; Prokleška, J.; Sechovský, V.; Tong, M. L. *Chem.—Eur. J.* **2013**, *19*, 13504−13510. (i) Guo, F. S.; Chen, Y. C.; Liu, J. L.; Leng, J. D.; Z.-S. Meng, Z. S.; Vrábel, P.; Orendáč, M.; Tong, M. L. *Chem. Commun.* **2012**, *48*, 12219−12221. (j) Sibille, R.; Mazet, T.; Malaman, B.; M. François, M. *Chem.—Eur. J.* **2012**, *18*, 12970−12973. (k) Biswas, S.; Adhikary, A.; Goswami, S.; Konar, S. *Dalton Trans.* **2013**, *42*, 13331−13334. (l) Goswami, S.; Adhikary, A.; Jena, H. S.; Konar, S. *Dalton Trans.* **2013**, *42*, 9813−9817. (m) Lorusso, G.; Sharples, J. W.; Palacios, E.; Roubeau, O.; Brechin, E. K.; Sessoli, R.; Rossin, A.; Tuna, F.; McInnes, E. J. L.; Collison, D.; Evangelisti, M. *Adv. Mater.* **2013**, *25*, 4653−4656. (n) Hou, Y. L.; Xiong, G.; Shi, P. F.; Cheng, R. R.; Cui, J. Z.; Zhao, B. *Chem. Commun.* **2013**, *49*, 6066−6068.

(10) (a) Titos-Padilla, S.; Ruiz, J.; Herrera, J. M.; Brechin, E. K.; Wersndorfer, W.; Lloret, F.; Colacio, E. *Inorg. Chem.* **2013**, *52*, 9620−9626. (b) Ehama, K.; Ohmichi, Y.; Sakamoto, S.; Fujinami, T.; Matsumoto, N.; Mochida, N.; Ishida, T.; Sunatsuki, Y.; Tsuchimoto, M.; Re, N. *Inorg. Chem.* **2013**, *52*, 12828−12841. (c) Zhang, P.; Zhang, L.; Lin, S. Y.; Tang, J. *Inorg. Chem.* **2013**, *52*, 6595−6602.

(11) (a) Liu, J. L.; Yuan, K.; Leng, J. D.; Ungur, L.; Wernsdorfer, W.; Guo, F. S.; Chibotaru, L. F.; Tong, M. L. *Inorg Chem.* **2012**, *51*, 8538−8544. (b) Lin, P. H.; Sun, W. B.; Tian, Y. M.; Yan, P. F.; Ungur, L.; Chibotaru, L. F.; Murugesu, M. *Dalton Trans.* **2012**, *41*, 12349−12352. (c) Leng, J. D.; Liu, J. L.; Zheng, Y. Z.; Ungur, L.; Chibotaru, L. F.; Guo, F. S.; Tong, M. L. *Chem Commun.* **2013**, *49*, 158−160. (d) Li, Q. W.; Liu, J. L.; Jia, J. H; Leng, J. D.; Lin, W. Q.; Chen, Y. C.; Tong, M. L. *Dalton Trans.* **2013**, *42*, 11262−11270. (e) Pointillart, F.; Le

Guennic, B.; Golhen, S.; Cador, O.; Maury, O.; Ouahab, L. *Chem. Commun.* **2013**, *49*, 615−617.
(12) (a) Bünzli, J. −C. G. *Chem. Rev.* **2010**, *110*, 2729−2755. (b) Faulkner, S.; Pope, S. J. A.; Burton-Pye, B. P. *Appl. Spectrosc. Rev.* **2005**, *40*, 1−31. (c) Lin, S. *Chem. Soc. Rev.* **2004**, *33*, 445−61.
(13) (a) Colacio, E.; Ruiz, J.; Mota, A. J.; Palacios, M. A.; Cremades, E.; Ruiz, E.; White, F. J.; Brechin, E. K. *Inorg. Chem.* **2012**, *51*, 5857−5868. (b) Colacio, E.; Ruiz, J.; Mota, A. J.; Palacios, M. A.; Ruiz, E.; Cremades, E.; Hänninen, M. M.; Sillanpää, R.; Brechin, E. K. *C. R. Chim.* **2012**, *15*, 878−888.
(14) Llunell, M.; Casanova, D.; Cirera, J.; Bofill, J. M.; Alemany, P.; Alvarez, S.; Pinsky, M.; Avnir, D. *SHAPE,* v1.1b; University of Barcelona and The Hebrew University of Jerusalem: Barcelona, 2005.
(15) Evangelisti, M.; Luis, F.; de Jongh, L. J.; Affronte, M. *J. Mater. Chem.* **2006**, *16*, 2534−2549 and references therein.
(16) Evangelisti, M.; Roubeau, O.; Palacios, E.; Camón, A.; Hooper, T. N.; Brechin, E. K.; Alonso, J. J. *Angew. Chem., Int. Ed.* **2011**, *50*, 6606−6609.
(17) Chilton, N. F.; Anderson, R. P.; Turner, L. D.; Soncini, A.; Murray, K. S. *J. Comput. Chem.* **2013**, *34*, 1164−1175.
(18) (a) Boulon, M.-E.; Cucinotta, G.; Luzon, J.; Degl'Innocenti, C.; Perfetti, M.; Bernot, K.; Calvez, G.; Caneschi, A.; Sessoli, R. *Angew. Chem., Int. Ed.* **2013**, *52*, 350−354. (b) Pointillart, F.; Guennic, B. L.; Cauchy, T.; Golhen, S.; Cador, O.; Maury, O.; Ouahab, L. *Inorg. Chem.* **2013**, *52*, 5978−5990. (c) Long, J.; Vallat, R.; Ferreira, R. A. S.; Carlos, L. D.; Almeida Paz, F. A.; Guari, Y.; Larionova, J. *Chem. Commun.* **2012**, *48*, 9974−9976. (d) Cucinotta, G.; Perfetti, M.; Luzon, J.; Etienne, M.; Car, P. E.; Caneschi, A.; Calvez, G.; Bernot, K.; Sessoli, R. *Angew.Chem., Int. Ed.* **2012**, *51*, 1606−1610. (e) Yamashita, K.; Miyazaki, R.; Kataoka, Y.; Nakanishi, T.; Hasegawa, Y.; Nakano, M.; Yamamura, T.; Kajiwara, T. *Dalton Trans.* **2013**, *42*, 1987−1990.
(19) (a) Ruiz, J.; Mota, A. J.; Rodríguez-Diéguez, A.; Titos, S.; Herrera, J. M.; Ruiz, E.; Cremades, E.; Costes, J. P.; Colacio, E. *Chem. Commun.* **2012**, *48*, 7916−7918. (b) Palacios, M. A.; Titos-Padilla, S.; Ruiz, J.; Herrera, J. M.; Pope, S. J.; Brechin, E. K.; Colacio, E. *Inorg. Chem.* **2014**, *53*, 1465−1474. (c) Bi, W. Y.; Lü, X. Q.; Chai, W. L.; Wei, T.; Song, J. R.; Zhao, S. S.; Wong, W. K. *Inorg. Chem. Commun.* **2009**, *12*, 267−271. (d) Xu, H. B.; Li, J.; Shi, L. X.; Chen, Z. N. *Dalton Trans.* **2011**, *40*, 5549. (c) Zhao, S.; Liu, X.; Feng, W.; Lü, X.; Wong, W. Y.; Wong, W. K. *Inorg. Chem. Commun.* **2012**, *20*, 41−45. (e) Bi, W. Y.; Lü, X. Q.; Chai, W. L.; Song, J. R.; Wong, W. Y.; Wong, W. K.; Jones, R. A. *J. Mol. Struct.* **2008**, *891*, 450−455. (f) Zhao, S.; Lü, X.; Hoy, A.; Wong, W. Y.; Wong, W. K.; Yang, X.; Jones, R. A. *Dalton Trans.* **2009**, 9595−9602. (g) Feng, W.; Hui, Y.; Wei, T.; Lü, X.; Song, J.; Chen, Z.; Zhao, S.; Wong, W. K.; Jones, R. A. *Inorg. Chem. Commun.* **2011**, *14*, 75−78. (h) Muller, G.; Maupin, C. L.; Riehl, J. P.; Birkedal, H.; Piguet, C.; Bünzli, J. C. G. *Eur. J. Inorg. Chem.* **2003**, 4065−4072. (i) Pasatoiu, T. D.; Tiseanu, C.; Madalan, A. M.; Jurca, B.; Duhayon, C. *Inorg. Chem.* **2011**, *50*, 5879−5889.
(20) (a) Sablayrolles, V.; Jubera, F.; Guillen, R.; Decourt, M.; Couzi, J. P.; Chaminade, A. Garcia *Opt. Commun.* **2007**, *280*, 103−109. (b) Jubera, V.; Artamenko, A.; Veber, P.; Velazquez, M.; Garcia, A. *ChemPhysChem.* **2011**, *12*, 1288−1293.
(21) Beeby, A.; Dickins, R. S.; Faulkner, S.; Parker, D.; Williams, J. A. G. *Chem. Commun.* **1997**, *15*, 1401−1402.
(22) Baldoví, J. J.; Cardona-Serra, S.; Clemente-Juan, J.; Coronado, E.; Gaita-Ariño, A.; Palii, A. *Inorg. Chem.* **2012**, *51*, 12565−12574.

■ NOTE ADDED AFTER ASAP PUBLICATION

This paper was published on the Web on March 5, 2014, with errors in Figure 5. The corrected version was reposted on March 7, 2014.